Supporting Information

Brady et al. 10.1073/pnas.1706197114

SI Materials and Methods

NMR Spectroscopy. Experiments were performed on Varian INOVA and Bruker Ascend III (11.7, 14.0, and 18.8 T) spectrometers equipped with triple-resonance gradient probes. NMR spectra were processed using the NMRPipe suite of programs (62) and analyzed using Sparky (63) and CCPN Analysis (64). The program FUDA (www.biochem.ucl.ac.uk/hansen/fuda/) was used to extract peak intensities from all multidimensional datasets.

Translational diffusion measurements. Translational diffusion coefficients for the small molecule probes in BSA, HEWL, $Ddx4_{14FtoA}$, and $Ddx4_{cond}$ were measured by recording a series of 2D ^{13}C-edited spectra at 30 °C using a pulse scheme that is similar to a previously published ^{15}N-edited experiment with ^{15}N and ^{13}C pulses interchanged (34). The constant delay diffusion period (after initial encoding of magnetization) was set to 100 ms. Diffusion coefficients of BSA (in BSA) and HEWL (in HEWL) were measured using a 1D water-suppressed longitudinal encode–decode (sLED) scheme (65), while diffusion measurements of ^{13}C-labeled Ig binding protein G (GB1) and heat shock protein 70 (HSC70; in BSA) were obtained as a series of 1D ^{13}C-edited spectra, 30 °C, with a diffusion period of 100 ms and an array of dephasing/rephasing gradients with strengths ranging from 10 to 31 G/cm (1-ms duration). Translational diffusion coefficients of Ddx4 in $Ddx4_{cond}$ were obtained from measurements on a sample where ∼1.5 mM U $-^{15}$ N,^{13} C-labeled protein was mixed with ∼13.5 mM unlabeled protein. A series of 1D ^{13}C-edited ^{1}H triple-quantum spectra, 30 °C, was recorded with a diffusion period of 400 ms and an array of bipolar dephasing/rephasing gradients (4-ms duration each) with strengths ranging from 4.5 to 40.5 G/cm (the pulse sequence is available on request). Translational diffusion coefficients of ^{15}N,^{13}C-labeled 4E-BP2 and $4E\text{-}BP2_{2x}$ were measured using the 1D version of the HNCO longitudinal encode–decode scheme of Fig. S5. The diffusion period was set to 400 ms, and an array of dephasing/rephrasing gradients with strengths ranging from 3.6 to 53.7 G/cm (2- to 2.5-ms duration) was used. Gradient strengths were calibrated by measuring the diffusion coefficient of the residual HDO in a D_2O sample using the known diffusion coefficient of water: 1.9×10^{-5} cm^2/s at 25 °C (66). In this case, a 1D longitudinal encode–decode pulsed field gradient NMR experiment was used (65).

Measurement of fractional water content. One-dimensional ^{1}H spectra were recorded on $Ddx4_{cond}$ samples, and the integrated water signals were compared with the corresponding integrals obtained from a spectrum recorded of buffer (the same buffer composition as used for $Ddx4_{cond}$). For phase-separated samples, it was ensured that the entirety of the probe coil was occupied by the condensed phase, thus avoiding contaminating signals from the more hydrated dilute phase. Spectra were recorded using both small flip angle ($\theta < 10°$) and $\theta = 90°$ pulses, with very similar results in both cases.

Dynamics measurements. NMR spin relaxation experiments (40) were performed at 18.8 T and 30 °C on a Bruker spectrometer equipped with a cryogenically cooled triple-resonance probe; ^{15}N{^{1}H} NOE values were determined from peak intensities in spectra obtained with/without 6-s proton saturation and a total delay of 14 s between scans (including saturation). ^{15}N R_1 relaxation rates were measured using relaxation delays of (10, 250, 500, 750); (10, 80, 160, 250, 360, 480, 620, 800); and (10, 250, 375, 500, 625, 750) ms for $Ddx4_{dil}$, $Ddx4_{14FtoA}$, and $Ddx4_{cond}$, respectively. ^{15}N $R_{1\rho}$ relaxation rates were recorded with spin lock (2-kHz) delays of (10, 20, 30, 40, 50, 60, 70, 90, 100, 120); (1, 7, 15, 23, 32, 42, 54, 66, 81, 98); and (10, 50, 100, 150) ms for $Ddx4_{dil}$ (∼7 mg/mL), $Ddx4_{14FtoA}$ (370 mg/mL), and $Ddx4_{cond}$ (380 mg/mL), respectively. More extensive $R_{1\rho}$ datasets were recorded for $Ddx4_{cond}$ on Varian spectrometers, and the R_2 rates obtained were essentially identical. R_2 values were calculated from experimental R_1 and $R_{1\rho}$ rates as detailed below.

Assignment of ILV residues. Each of the 12 Ile, Leu, and Val residues (4 Ile, 3 Leu, and 5 Val) in Ddx4 were substituted with Ala in a series of mutations that included I15A_V193A_L194A, V23A_I25A_L167A, L219A_V223A_I224A, V92A_L174A, and L186A. This led to unambiguous assignment of these residues in $Ddx4_{dil}$, and the assignments could then be transferred directly to $Ddx4_{14FtoA}$ and $Ddx4_{cond}$.

NOESY spectra. F_1 ^{13}C-filtered, F_2 ^{13}C-edited NOESY spectra (44) were recorded on samples prepared by mixing 10% (1 mM) ^{13}C-labeled Ddx4 with 90% unlabeled Ddx4 to probe intermolecular interactions in $Ddx4_{14FtoA}$ and $Ddx4_{cond}$. A concentration of 370 mg/mL was used for $Ddx4_{14FtoA}$, similar to $Ddx4_{cond}$ (380 mg/mL). The 3D (2D) spectra were recorded at 11.7 T (14.0 T) and 30 °C using a 150-ms mixing time. NOEs were assigned to a particular amino acid type only when there was unambiguous identification based on reported random coil chemical shift values by Wishart et al. (38).

Assignment of 4E-BP2 in $Ddx4_{cond}$. Backbone chemical shifts for 4E-BP2 (500 μM) dissolved in buffer composed of 20 mM NaPi, 100 mM NaCl, 5 mM TCEP, 1 mM Benzamadine, and 1 mM EDTA, pH 6.5 at 30 °C were obtained using HNCO, HN(CA)CO, CBCA(CO)NH, HNCACB, and HNN/HN(C)N experiments (67, 68). ^{1}H-^{15}N HSQC and HNCO experiments were collected for 250 μM 4E-BP2 in $Ddx4_{cond}$, 20 mM NaPi, 100 mM NaCl, 5 mM TCEP, 1 mM Benzamadine, and 1 mM EDTA, pH 6.5 at 30 °C, and assignments were transferred from 4E-BP2 in buffer to 4E-BP2 in $Ddx4_{cond}$. Approximately 55% of backbone and $^{13}C^{\beta}$ shifts could be assigned for 4E-BP2 in buffer (many peaks are weak or absent because of exchange with water), and 30% of the assignments in $Ddx4_{cond}$ could be obtained by transferring those in buffer.

Extraction of Relaxation Parameters. R_2 values were calculated from experimental R_1 and $R_{1\rho}$ rates according to (40)

$$R_2 = \frac{R_{1\rho} - R_1 \cos^2\theta}{\sin^2\theta}, \qquad \text{[S1]}$$

where $\theta = \tan^{-1}(\nu_{sl}/\Delta\nu)$, $\Delta\nu$ is the offset of the peak from the carrier frequency, and ν_{sl} is the strength of the spin lock field. The T_1, T_2 relaxation times and ^{15}N{^{1}H} NOE values can be expressed as (69)

$$\frac{1}{T_1} = d^2\left[J(\omega_H - \omega_N) + 3J(\omega_N) + 6J(\omega_H + \omega_N)\right] + c^2 J(\omega_N) \qquad \text{[S2]}$$

$$\frac{1}{T_2} = 0.5d^2\left[4J(0) + J(\omega_H - \omega_N) + 3J(\omega_N) + 6J(\omega_H) + 6J(\omega_H + \omega_N)\right] + \frac{1}{6}c^2\left[3J(\omega_N) + 4J(0)\right] \qquad \text{[S3]}$$

$$NOE = 1 + \left[\left(\frac{\gamma_H}{\gamma_N}\right) d^2\left\{6J(\omega_H + \omega_N) - J(\omega_H - \omega_N)\right\} T_1\right], \qquad \text{[S4]}$$

where $d^2 = 0.1[\mu_0 h\gamma_H\gamma_N/8\pi^2]^2 < r_{NH}{}^{-3} >^2$, $c^2 = 2/15(\omega_N{}^2)(\sigma_\parallel - \sigma_\perp)^2$; μ_0 is the permeability of free space; γ_j and ω_j are the gyromagnetic ratio and nuclear Larmor frequency of spin j, respectively; h is Planck's constant; r_{NH} is the length of the amide bond (1.02 Å); and $\sigma_\parallel$ and $\sigma_\perp$ are the parallel and perpendicular components of the assumed axially symmetric ^{15}N chemical shift tensor [$(\sigma_\parallel - \sigma_\perp) = -172$ ppm], respectively (70). The spectral density, $J(\omega)$, in Eqs. **S2–S4** is given by

$$J(\omega) = \frac{S^2\tau_c}{(1+(\omega\tau_c)^2)} + \frac{(1-S^2)\,\tau}{(1+(\omega\tau)^2)}, \qquad \textbf{[S5]}$$

where $\tau^{-1} = \tau_c^{-1} + \tau_e^{-1}$; τ_c and τ_e are residue-specific correlation times describing overall tumbling and rapid motion of the amide bond vector, respectively; and S^2 is the square of the order parameter. Values of S^2, τ_c, and τ_e were extracted by fitting experimental T_1, T_2, and ^{15}N{^{1}H} NOE values using Eqs. **S2–S5**, and the product $S^2\tau_c$, averaged over all residues, is reported in Table S1.

Fitting of Translational Diffusion Measurements. Signal intensities in translational diffusion experiments are dependent on the gradient strength (G) and the diffusion coefficient (D) of the probe of interest according to the expression

$$\frac{I}{I_0} = \exp(-eG^2), \qquad \textbf{[S6]}$$

where e is a constant that depends, among other things, on D. Values of the hydrodynamic radii of probe molecules in Fig. 6 (x axis), R_p, were measured using samples containing a small amount of acetate as a reference, so that $R_p = e_{acetate,buff}/e_{probe,buff} \cdot R_{p,acetate}$, where $R_{p,acetate}$ = 2.24 Å (71), and the subscript *buff* emphasizes the fact that the diffusion measurements were made in buffer samples (as opposed to proteinaceous samples). In this manner, R_p values for the small molecule probes used in this study that included ^{13}C-labeled methanol, 1-^{13}C ethanol, 2-^{13}C acetate, 2-^{13}C isopropanol, 2-^{13}C glycerol, 1-^{13}C ribose, ^{13}C glucose, and ^{13}C sucrose as well as GB1, HEWL, BSA, and HSC70 protein probes, were obtained. The diffusion of small molecules in Ddx4$_{cond}$ (380 mg/mL), Ddx4$_{14FtoA}$ (212 mg/mL), and BSA (250 mg/mL) was measured at concentrations of 2 and ∼10 mM. There was no appreciable change between concentrations, indicating no interactions with the protein crowding agent. Diffusion constants of small molecule and protein probes dissolved in HEWL, BSA, Ddx4$_{14FtoA}$, Ddx4$_{24RtoK}$, and Ddx4$_{cond}$ were obtained from expressions like those in Eq. **S6** and subsequently analyzed as described in the text.

Diffusion of Proteins Within Ddx4$_{cond}$. We have measured diffusion coefficients for 4E-BP2 and 4E-BP2$_{2x}$ in Ddx4$_{cond}$ (380 mg/mL) using the pulse scheme illustrated in Fig. S5. A major complication in measuring spectra of tracer proteins in Ddx4$_{cond}$ has been residual signal that arises from the very high concentration of Ddx4 in the phase-separated state (10 mM), although it is unlabeled. For example, at typical concentrations of 5% mole fraction-labeled tracer, ∼20% of the signal in a ^{13}C-edited dataset originates from Ddx4 that is readily observed in spectra (especially considering that Ddx4 is unfolded). Notably, we can also record very high-quality natural abundance ^{15}N-edited spectra of Ddx4 that would interfere with any measurements of tracer proteins that use a selection based on ^{15}N. We have, therefore, chosen to develop an HNCO-based longitudinal encode–decode sequence that makes use of combined ^{15}N,^{13}C filtering to eliminate Ddx4 from spectra. Of particular importance is the coherence transfer selection from ^{15}N to ^{1}H at the end of the pulse sequence that was achieved using gradients (B and B′ in Fig. S5), since on our spectrometers (and in our noisy magnetic environment), we were not able to eliminate spurious peaks derived from Ddx4 based on phase cycling alone.

Fits of Phase Diagrams to Simple Flory–Huggins Theory. The free energy of mixing per unit volume (lattice site) for a solution comprising a polymer chain (protein) and solvent (water), denoted here as ΔF_{mix}, may be described approximately according to the mean field Flory–Huggins theory by

$$\frac{\Delta F_{mix}}{kT} = \frac{\phi}{N_1}\ln\phi + \frac{(1-\phi)}{N_2}\ln(1-\phi) + \chi\phi(1-\phi), \qquad \textbf{[S7]}$$

where ϕ and $1-\phi$ are the volume fractions of protein and water, respectively; N_1 and N_2 are the numbers of lattice sites occupied by protein (number of amino acids) and water, respectively, with $N_1 = 241$ (for Ddx4) and $N_2 = 1$ in the case of interest; and χ is a temperature-dependent interaction parameter, $\chi = A + B/T$. For simplicity, unlike approaches in more involved treatments (59), here we assume that each lattice site is fully occupied by either a solvent molecule or a protein residue. The logarithmic terms in Eq. **S7** describe the purely entropic contributions to the mixing energy. The value of ϕ is calculated according to

$$\phi = \frac{c}{\rho}, \qquad \textbf{[S8]}$$

where c is the protein concentration in milligrams per milliliter, and ρ is the protein density. Following standard treatments (2, 59), if the free energy function ΔF_{mix} is convex throughout, then the solution will be mixed at all compositions. However, if the landscape contains concave features (Fig. S7), then the system can phase separate. The volume fraction of protein in the dilute and concentrated sides of the phase diagram, ϕ' and. ϕ'', respectively, can be calculated from the following relations (72):

$$\left(\frac{\partial\Delta F_{mix}}{\partial\phi}\right)_{\phi=\phi'} = \left(\frac{\partial\Delta F_{mix}}{\partial\phi}\right)_{\phi=\phi''} \qquad \textbf{[S9.1]}$$

$$\frac{\Delta F_{mix}(\phi') - \Delta F_{mix}(\phi'')}{\phi' - \phi''} = \left(\frac{\partial\Delta F_{mix}}{\partial\phi}\right)_{\phi=\phi' or \phi''}, \qquad \textbf{[S9.2]}$$

where

$$\left(\frac{\partial\Delta F_{mix}}{\partial\phi}\right) = kT\left[\frac{\ln\phi}{N_1} + \frac{1}{N_1} - \frac{\ln(1-\phi)}{N_2} - \frac{1}{N_2} + \chi(1-2\phi)\right], \qquad \textbf{[S10]}$$

yielding

$$\chi = A + \frac{B}{T} = \frac{\frac{1}{N_1}\ln\left(\frac{\phi''}{\phi'}\right) + \frac{1}{N_2}\ln\left(\frac{1-\phi'}{1-\phi''}\right)}{2(\phi'' - \phi')}. \qquad \textbf{[S11]}$$

Thus, if the phase diagram is determined experimentally, $\chi(T)$ is established from the measured ϕ' and ϕ'' values by obtaining the best fit A and B values (Fig. S7 *A* and *B*). The fitted phase diagram (solid line in Fig. S7*D*) is then obtained by calculating the free energy function for each χ as in Fig. S7*C*. Values of ϕ' and ϕ'' are obtained from the free energy profile by enforcing Eq. **S9** (Fig. S7*C*). After these are determined, the phase diagram is calculated. In the fits of the salt-dependent Ddx4$_{cond}$ phase diagrams, each salt series was considered independently, and the density of Ddx4$_{cond}$ was a fitted parameter (ρ = 1587 mg/mL) that was optimized to give the best fit over the complete salt range.

Estimating the Effective Attractive Energy Between Ddx4 Chains Using Simple Flory–Huggins Theory. The Flory–Huggins expression ΔF_{mix} in Eq. **S7** for the free energy per unit volume implies that $\Delta F_{mix}/\phi$ is the free energy per amino acid, because the probability of any volume being occupied by a residue is ϕ. It

follows that the interaction energy component of $\Delta F_{mix}/\phi$ is equal to $kT\chi(1-\phi)$ and that the configurational entropic component is $kT(\ln\phi)/N_1 + kT[(1-\phi)/\phi]\ln(1-\phi)$, where we have used $N_2 = 1$ as stated above. Fitting the simple Flory–Huggins model to the data in Fig. 1 for Ddx4 at [NaCl] = 100, 300 mM and $Ddx4_{CS}$ at [NaCl] = 100 mM yields a condensed-phase volume fraction $\phi \approx 0.2$ for all three cases (0.22, 0.17, and 0.16, respectively). At $T = 300$ K, the $kT\chi$ values for these three systems are 0.362, 0.352, and 0.350 kcal mol^{-1}, respectively; hence, the corresponding average total interaction energies per residue are $kT\chi(1-\phi) = 0.283$, 0.291, and 0.295 kcal mol^{-1}, respectively [i.e., the average interaction energy per residue in phase-separated Ddx4 (and variants) is ≈0.3 kcal mol^{-1}]. This is much weaker than the ≈1.5 kcal mol^{-1} per residue for protein folding. The latter follows from an average loss of 1.4 kcal mol^{-1} per residue in the conformational entropic component of free energy (57) and a decrease of 0.05 to 0.12 kcal mol^{-1} per residue in overall free energy on folding of globular proteins (58). The mixing entropies per residue of the condensed phase of the three sequences/salt concentrations considered (see above) are given by their corresponding free energies $kT(\ln\phi)/N_1 + kT[(1-\phi)/\phi]\ln(1-\phi) \approx -0.88$, -0.91, and $-0.92\ kT$, respectively. The Flory–Huggins mixing entropy is defined to be relative to the completely demixed scenario ($\phi = 1$), in which each residue gains about $kT\ln e = kT = 0.59$ kcal mol^{-1} of free energy from the conformational entropy component relative to an unrestrained conformer (73). Taken together, the free energy contributions per residue from conformational entropy in the Ddx4 condensed phases considered above are only 0.12, 0.09, and 0.08 kT or 0.083, 0.062, and 0.055 kcal mol^{-1}, respectively, higher than for the corresponding unrestrained conformer. The configurational entropy predicted by the simple Flory–Huggins theory is thus reasonable, because a high degree of conformational freedom is expected for a condensed phase with $\phi \approx 0.2$.

$Ddx4_{cond}$ Does Not Form Irreversible Aggregates or Fibrils. Much has been made in the literature of droplet "maturation" and the possibility of the phase-separated state acting as a path toward aggregation or fibrillation (23, 32, 33, 74). To explore these possibilities for $Ddx4_{cond}$, we performed Thioflavin T (ThT) fluorescence and negative stain EM experiments on samples that had been incubated for extended periods (up to 3 wk). No evidence was found for irreversible aggregation or amyloid fibril formation. Negative stain EM was performed on samples of $Ddx4_{cond}$, which were incubated at 30 °C for 2 d. Since the concentration of protein in $Ddx4_{cond}$ is orders of magnitude greater than that required for EM, samples were diluted 1,000- and 10,000-fold into buffer containing 20 mM NaPi, 100 mM NaCl, and 10 mM DTT, pH 6.5 for final protein concentrations of ∼0.4 and ∼0.04 mg/mL, respectively. As has been previously observed (in the text), the condensed protein phase mixed readily on dilution into buffer, forming a single transparent and homogeneous phase, and the resulting electron micrographs (Fig. S1 *A* and *B*) showed no evidence of aggregation or fibril formation. Additionally, we measured ThT fluorescence on a sample of Ddx4, which had been incubated at room temperature for >3 wk. Fresh DTT (20 mM) was added to the sample to reduce cysteine side chains (see below). The ratio of ThT fluorescence with and without Ddx4 was recorded at four concentrations of ThT (50, 100, 150, and 200 μM), keeping the amount of Ddx4 constant (Fig. S1*C*). Fluorescence excitation (emission) of ThT was recorded at 450 (482) nm using a SpectraMax i3x (Molecular Devices) Microplate Reader system. No significant increase in fluorescence was observed for different concentrations of ThT, in contrast to the extent of ThT fluorescence in the presence of amyloid-β (Aβ) fibrils (KLVFFAE sequence; donation of Simon Sharpe, Hospital for Sick Children, Toronto, ON, Canada). There is thus no evidence for Ddx4 fibril formation. Notably, however, $Ddx4_{cond}$ does form a gel-like state after an extended period of incubation (3 wk) at room temperature (20 mM NaPi, 100 mM NaCl, 20 mM DTT, pH 6.5). This can be primarily attributed to the oxidation of cysteine side chains, since addition of fresh reducing agent readily liquefied the gel. It should be noted that we have been careful to use TCEP as reducing agent in NMR samples because of its greatly increased stability compared with DTT. We have not observed any evidence for irreversible maturation of Ddx4 droplets, as samples can always be redissolved into low-salt buffer (20 mM NaPi, 100 mM NaCl, 10–20 mM DTT), while phase-separated samples provide high-quality NMR spectra for weeks.

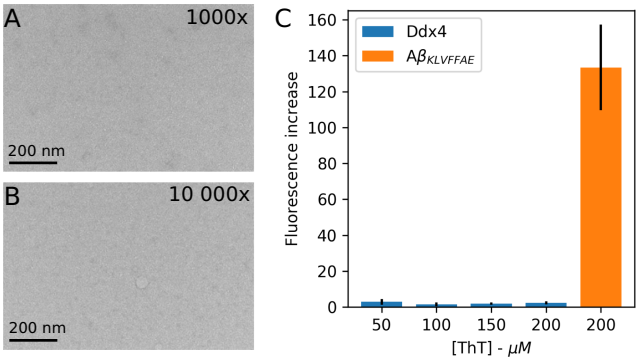

Fig. S1. Negative stain EM of Ddx4. The 1,000- (*A*) and 10,000-fold (*B*) dilutions of $Ddx4_{cond}$ into 20 mM NaPi, 100 mM NaCl, and 10 mM DTT, pH 6.5. Samples were prepared by staining with uranyl acetate [2% (wt/vol) solution] on Cu/Rh 400 mesh grids, with a fresh continuous carbon layer applied over a nitrocellulose film. Images were taken on a Tecnai F20 microscope (FEI) at a nominal magnification of 25,000×, and defocus ranged from 0.5 to 1.0 μm. $Ddx4_{cond}$ readily dissolved into buffer on dilution below the concentration at which phase separation occurs. Extensive searching of grids revealed no signs of aggregation or fibril formation. Samples were incubated for 2 d before imaging. (*C*) Ratio of ThT fluorescence with and without Ddx4 or Aβ fibrils. Error bars represent one SD from at least six replicates. Fluorescence excitation (emission) of ThT was recorded at 450 (482) nm using a SpectraMax i3x Microplate Reader system (Molecular Devices). The Ddx4 sample had been incubated at room temperature for 3 wk before measurement.

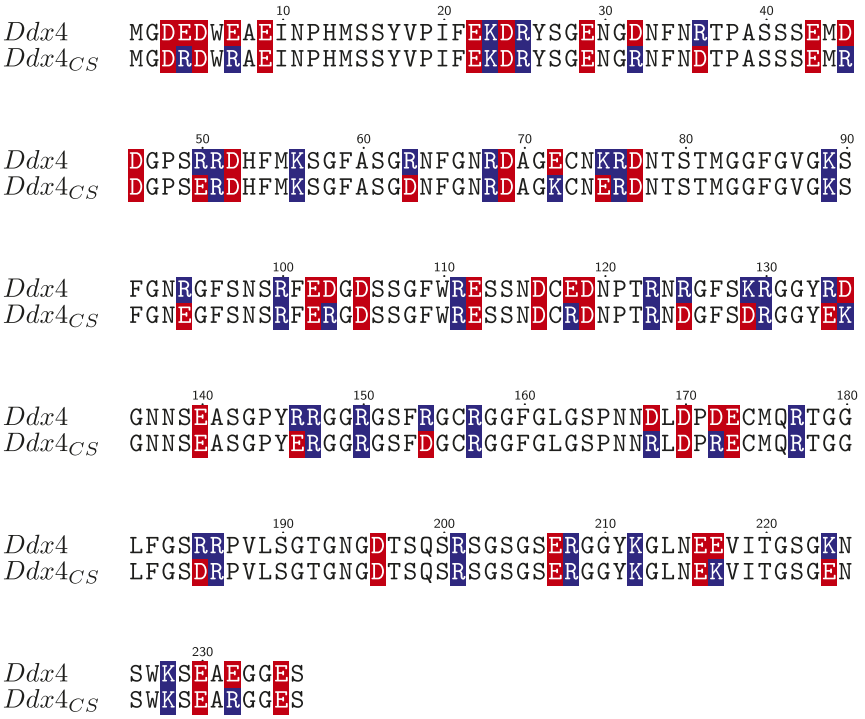

Fig. S2. Sequence alignment showing positions of positive (blue) and negative (red) charged residues for WT Ddx4 and Ddx4$_{CS}$. A metric, κ, has been developed to describe the linear distribution of charges in a sequence (75), with $\kappa = 1$ for complete segregation of charge and $\kappa = 0$ for no charge asymmetry. Using this metric, κ values of 0.272 and 0.069 are obtained for WT Ddx4 (15) and Ddx4$_{CS}$, respectively, indicating that Ddx4$_{CS}$ has a significantly more even distribution of charged residues than Ddx4.

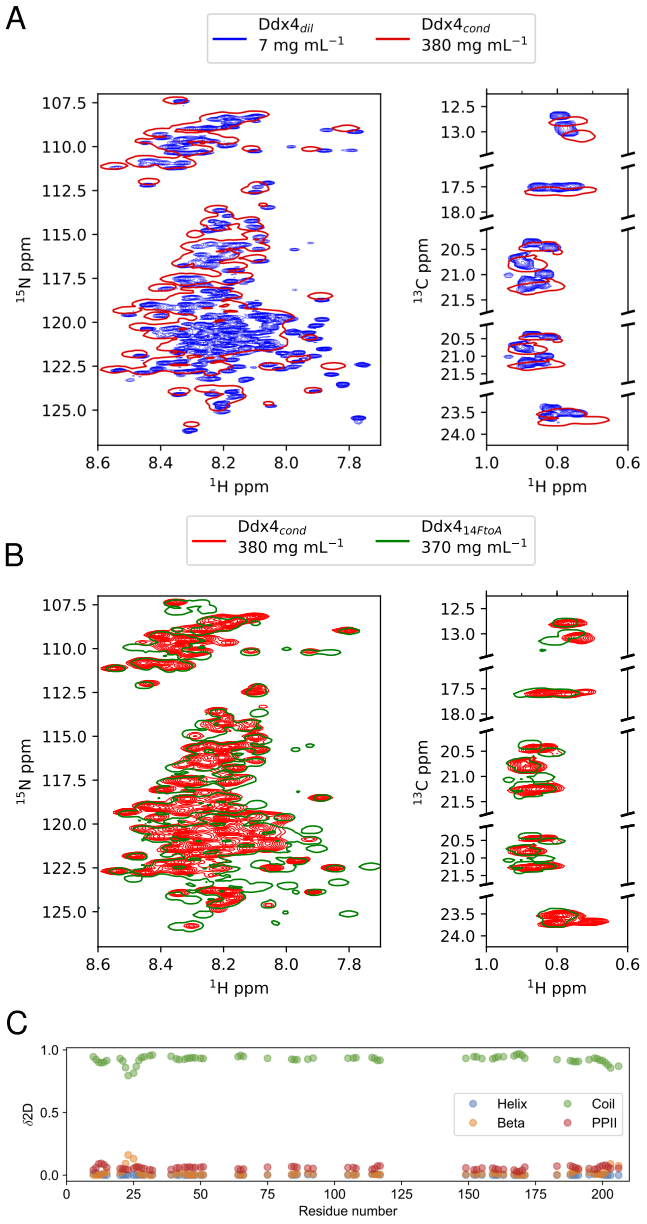

Fig. S3. (*A* and *B*) Overlays of ^{1}H-^{15}N HSQC spectra of Ddx4$_{cond}$ with Ddx4$_{dil}$ (*A*) and Ddx4$_{cond}$ with Ddx4$_{14FtoA}$ (*B*). All spectra were recorded at 18.8 T and 30 °C. (*C*) δ2D scores (76) as a function of residue based on available backbone assignments for Ddx4 (PPII is polyproline II helix secondary structure propensity). $^{13}C\alpha$, $^{13}C\beta$, and carbonyl shifts were used for each residue. Values close to one indicate a high propensity to form the indicated secondary structural element. The average coil propensity across the sequence was calculated to be 0.92.

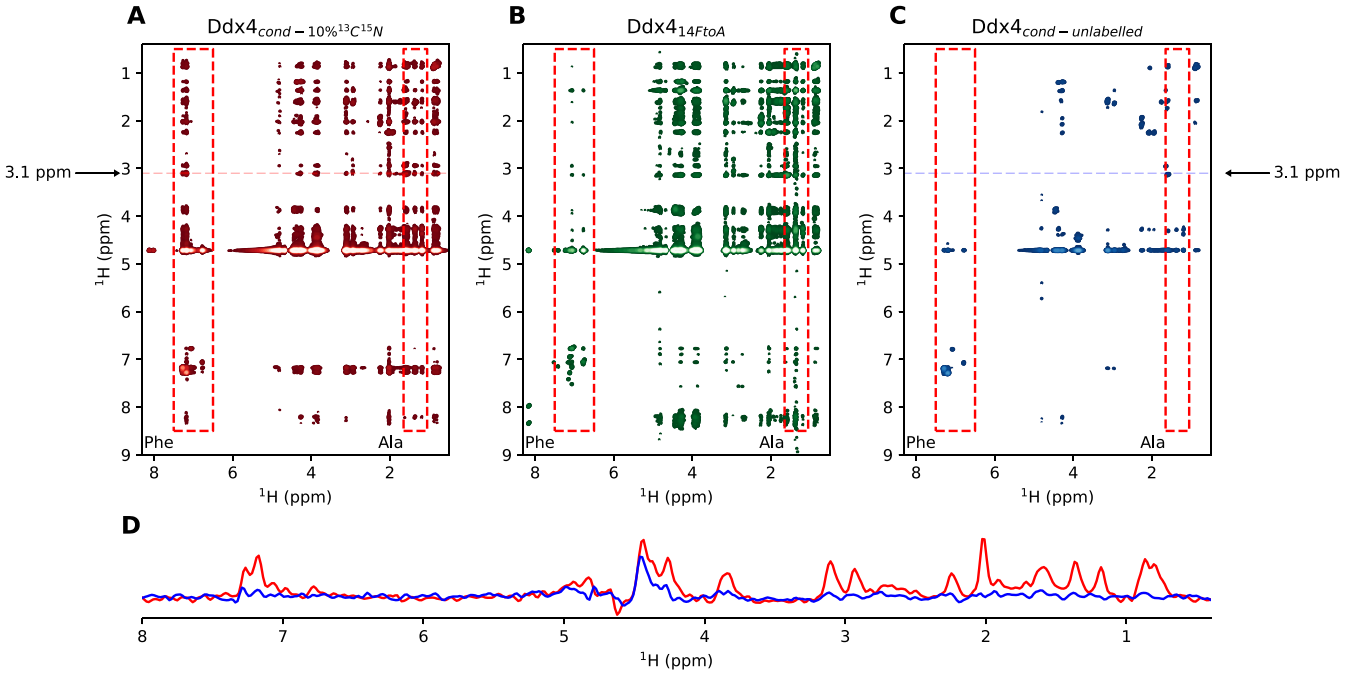

Fig. S4. Measurement of intermolecular NOEs in samples of $Ddx4_{cond}$ (*A*; 380 mg/mL; red) and $Ddx4_{14FtoA}$ (*B*; 370 mg/mL; green) as described in the text at 30 °C, 14. 1 T, and mixing time = 150 ms. Samples were prepared by mixing 10% (1 mM) ^{15}N, ^{13}C-labeled Ddx4 with 90% unlabeled Ddx4. As expected, more NOE peaks are present in the aromatic region of the $Ddx4_{cond}$ spectrum and in the Ala region of the $Ddx4_{14FtoA}$ spectrum. Ala H^{β} region at 1.35 ± 0.30 ppm and Phe aromatic proton region, 7.0 ± 0.5 ppm, are highlighted (red outline). It is noteworthy that a comparison of NOE intensities can only be qualitative as differences in dynamics between molecules in $Ddx4_{cond}$, and $Ddx4_{14FtoA}$ (Fig. 4) will affect cross-relaxation efficiencies. As a control, a sample of 100% unlabeled Ddx4 was also prepared (380 mg/mL), from which the spectrum of *C* (blue) was obtained. For comparison, horizontal traces (*D*; 3.1 ppm in F_1; marked by dashed lines in *A* and *C*) are illustrated. These show a very low level of intramolecular cross-peaks arising from natural abundance ^{13}C that, therefore, do not significantly affect our conclusions. Spectra are displayed at the same contour level.

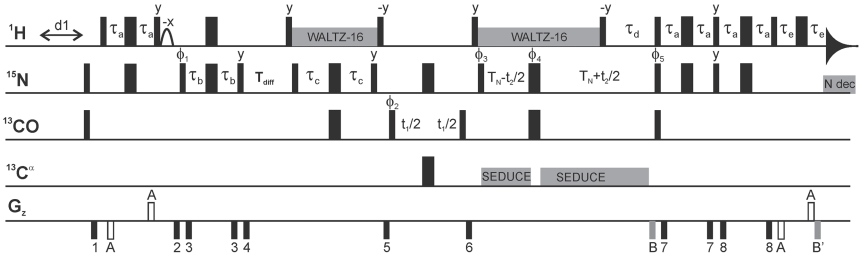

Fig. S5. HNCO-based longitudinal encode–decode scheme for measurement of diffusion of ^{15}N,^{13}C-labeled proteins. Although a 3D version of the experiment is illustrated here, all diffusion experiments in this work were performed in "1D" mode, where $^{13}C^{\alpha}$ and ^{15}N pulses in the center of the t_1 period were eliminated and replaced by a ^{13}CO pulse and $t_1 = t_2 = 0$. Narrow and wide rectangles correspond to 90° and 180° pulses, respectively, applied along the *x* axis unless otherwise indicated. ^{1}H decoupling is achieved using a 6-kHz WALTZ-16 decoupling element (77). The ^{1}H, ^{15}N, and ^{13}C carriers are placed at water, 119 and 176 ppm, respectively for the duration of the experiment. $^{13}C^{\alpha}$ and ^{13}CO rectangular pulses are applied with fields of $\zeta/\sqrt{3}$ Hz (180°) or $\zeta/\sqrt{15}$ Hz (90°), where ζ is the frequency difference in hertz between the centers of the $^{13}C^{\alpha}$ (58 ppm) and ^{13}CO (176 ppm) spectral regions (78). $^{13}C^{\alpha}$ decoupling during t_2 is achieved using an ∼1-kHz SEDUCE element (79). Note that, in 1D mode, this element is not required. Delays are $\tau_a = 2.3$ ms, $\tau_b = 2.7$ ms, $\tau_c = 12.4$ ms, $\tau_d = 5.5$ ms, $\tau_e = 3.0$ ms, and $T_N = 12.4$ ms. The phase cycle is $\phi_1 = 4(x), 4(-x)$, $\phi_2 = 2(x), 2(-x)$, $\phi_3 = x, -x$, $\phi_4 = 8(x), 8(-x)$, $\phi_5 = x$, and rec = $x, 2(-x), x, -x, 2(x), -x$. Gradient levels and durations (gauss per centimeter; milliseconds) are g1 = (16; 0.5), g2 = (30; 2.0), g3 = (−10; 0.4), g4 = (24; 0.6), g5 = (40; 0.75), g6 = (24; 0.6), g7 = (10,0.3), g8 = (20; 0.2), gA = diffusion encoding/decoding gradient (arrayed, typically 2 ms), gB = (60; 1.25), and gB′ = (59.2; 0.125). Quadrature in F_1 is achieved via States-TPPI (time proportional phase incrementation) (80) of ϕ_2. Quadrature in F_2 is achieved using the gradient enhanced sensitivity method (81, 82), whereby separate datasets are recorded with (ϕ_5, gB) and ($\phi_5 + 180°$, −gB). For each t_1 increment, ϕ_2 and the receiver phase are incremented by 180° (80).

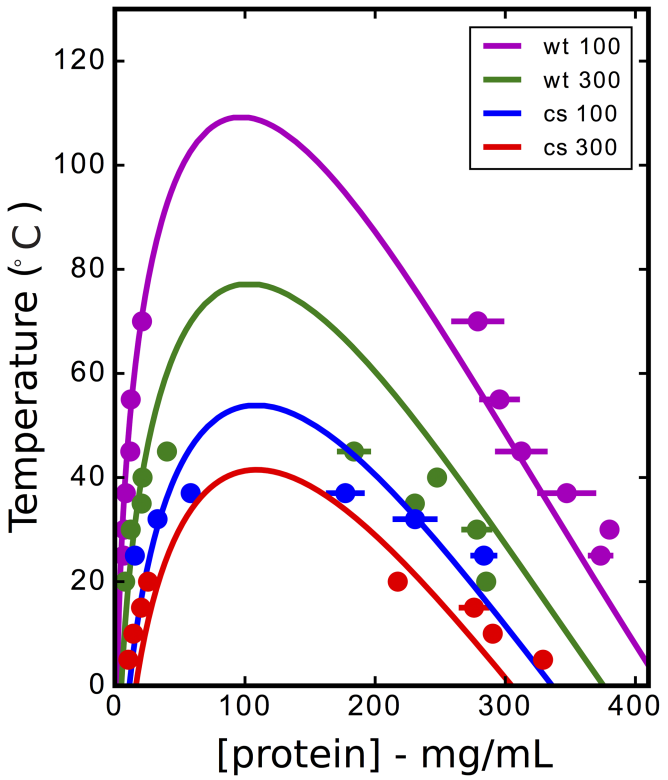

Fig. S6. Experimental data (circles) compared with phase diagrams (solid curves) predicted by the random phase approximation (RPA) + Flory-Huggins (FH) theory of Lin et al. (30, 59). To provide a physical account for sequence-dependent phase behavior, only three parameters, namely ϵ_r and two parameters for a global χ, are used to describe all coexistence curves (i.e., unlike the simple Flory–Huggins approach used for Fig. 1, different coexistence curves here are not fitted using different χ parameters). The parameters are optimized by simultaneously fitting to the 100 mM NaCl data of WT Ddx4 and charge-scrambled Ddx4_{CS} (magenta and blue curves, respectively). Results shown indicate that this set of fitted parameters affords a reasonably accurate prediction for the two sets of 300 mM NaCl data that were not used to determine the fitting parameters. This comparison shows that the RPA + FH theory successfully rationalizes the difference between WT and charge-scrambled Ddx4 caused by their different charge patterns. Salt dependence is also considered by the same theory, but the discrepancies with experiment increase with increasing salt concentrations. The fitting procedure used here is similar to that for the simple Flory–Huggins model in the text, except an additional RPA contribution from electrostatic free energy (30, 59) is included in this case. In the notation of refs. 30 and 59, the size of an amino acid residue in this calculation is taken to be $r = 3.72$ times that of a water molecule, and the fitted parameters are $\epsilon_r = 61.5$, $\epsilon_h = 0.0754$, and $\epsilon_s = 0.415$.

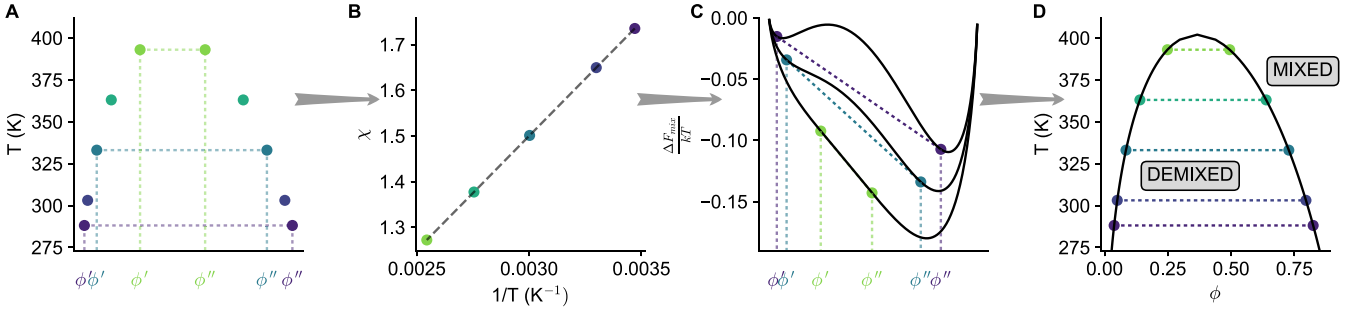

Fig. S7. Schematic illustrating fitting of phase diagrams. (*A*) Experimental phase diagram. At each temperature, volume fractions of protein from dilute and concentrated regions of demixed solutions are measured to give the curve in *A*. Values of ϕ' and ϕ'' at each temperature, *T*, are used to calculate the best fit $\chi(T)$ in *B* using Eq. **S11**. Values of $\chi(T)$ are then used to generate energy landscapes (*C*) (Eq. **S7**), from which a continuous set of $[\phi'(T), \phi''(T)]$ pairs is calculated by enforcing Eq. **S9** that, in turn, generates the solid curve in *D*.

Table S1. Rotational and translational diffusion of Ddx4

Protein	Concentration	MW(kDa)	D(cm^2/s)*	R_H†	$<S^2\tau_c>$‡ (ns)
Ubiquitin§		8.5	2.0×10^{-6} ($\pm$0.1)	15.7	3.3
$Ddx4_{dil}$	7 mg/mL¶	25.8	8.8×10^{-7} ($\pm$0.2)	31.6	1.5($\pm$0.5)
$Ddx4_{14FtoA}$	D_0#	24.8	9.0×10^{-7} ($\pm$0.1)	30.9	‖
$Ddx4_{14FtoA}$	250 mg/mL	24.8	3.5×10^{-8} ($\pm$0.1)	**	2.4($\pm$0.8)
$Ddx4_{14FtoA}$	370 mg/mL	24.8	9.2×10^{-9} ($\pm$0.9)	**	4.8($\pm$1.5)
$Ddx4_{cond}$	380 mg/mL	25.8	7.5×10^{-9} ($\pm$0.4)	**	8.5($\pm$3)
$Ddx4_{cond}$††	440 mg/mL	25.8	5.4×10^{-9} ($\pm$0.4)	**	10.4($\pm$4)

D_0, concentration extrapolated to 0; MW, molecular mass.

*Measured by pulsed field gradient NMR as described in *SI Materials and Methods* (30 °C).

†Hydrodynamic radius (R_H) calculated from measured diffusion coefficient in buffer along with diffusion of acetate (30 °C) (*SI Materials and Methods*).

‡Product of square of order parameter for backbone amide, S^2, and residue-specific overall tumbling time, τ_C, averaged over residues for which data is available (30 °C).

§$<S^2\tau_C>$ data from refs. 57 and 58.

¶Sample obtained from the dilute phase of phase-separated Ddx4.

#Extrapolated from self-diffusion data as a function of concentration to zero concentration.

‖Relaxation data not measured.

**Hydrodynamic radius cannot be accurately extracted from diffusion measurements on concentrated samples because of elevated viscosity. All estimates of R_H make use of dilute Ddx4 samples.

††A lower NaCl concentration was used (7.5 mM) relative to all other Ddx4 samples to achieve a higher protein concentration in the condensed phase.

Table S2. Summary of driving forces for phase separation of Ddx4

Parameter	Effect on phase separation	Evidence	Probable cause
Loss of Arg	Decreases propensity	$Ddx4_{24RtoK}$	Loss of potential π–π/cation–π interactions abrogates ability to phase separate (in the text)
Loss of Phe	Decreases propensity	$Ddx4_{14FtoA}$	Loss of potential π–π/cation–π interactions abrogates ability to phase separate (in the text)
Charge segregation	Increases propensity	$Ddx4_{CS}$	Scrambling of segregated charges reduces propensity to phase separate (Fig. 1)
Salt	Decreases propensity	Phase diagrams	Increasing salt concentration reduces critical temperature at which phase separation occurs
Temperature	Decreases propensity	Phase diagrams	Increasing temperature disfavors phase separation of Ddx4 (UCST)